Using audio-frequency waves at porous and rough surfaces

K. Attenborough, H.-C. Shin, I. Bashir et S. Taherzadeh
The Open University, Faculty of Mathematics, Computing and Technology, Walton Hall, MK7 6AA
Milton Keynes, UK
keith.attenborough@open.ac.uk

Applications of acoustic-to-seismic (A/S) coupling and surface waves are described. Laser Doppler Vibrometer measurements of the spectra of soil particle motion resulting from insonification of the soil surface can be modelled with Biot-Stoll Theory and an optimised fitting procedure enables deductions of the variation of rigidity modulus with depth. Examples are shown of comparisons between A/S-deduced soil strength profiles and those measured using a penetrometer. The second application concerns the design of rough surfaces for noise control. Surface waves are created as sound propagates from a point source close to a rough acoustically-hard surface composed from periodically-spaced rectangular strips and are accompanied by diffraction-assisted ground effect. When the edge-to-edge spacing is substantially smaller than the strip height these surfaces may be regarded as locally-reacting rigid-framed hard-backed porous layers with an effective depth slightly larger than the strip height. When the spacing is comparable to the strip height or greater the surfaces behave as periodically-rough surfaces. Outdoor measurements over rough surfaces composed of bricks indicate that generation and attenuation of surface waves at rough ground surfaces can be used to reduce noise from surface transport.

Introduction

1.1 Deducing soil rigidity

Soil structure, moisture content and strength have profound effects on plant growth. Measurements of soil physical condition have traditionally been through fairly laborious invasive means: for example, by analysis of extracted samples or by making a series of invasive readings in the field with a penetrometer which measures the resistance to penetration of a steel spike mounted on a specially designed jig. Soils are regarded as porous elastic (poro-elastic) media, and sub-surface wave propagation can be used as an indication of the soil status. Such propagation can be initiated non-invasively by sources of airborne sound which cause motion of air particles in the pores and of soil particles in the pore walls, in other words, the granular framework of the soil. The spectrum of the ratio of the surface soil particle velocity to the incident pressure is known as the acoustic to seismic (A/S) coupling spectrum. Measurements of A/S coupling in soils and of the interference between soil surface-reflected and incident sounds can be exploited to estimate the pore-related and elastic/seismic properties of soils through non-invasive means. Previous measurements of A/S coupling on unconsolidated sand have been made in a laboratory using a laser Doppler vibrometer (LDV) and a microphone [1]. Measurements of A/S coupling using an LDV have been used to detect buried objects in the field, notably landmines [2].

Outdoor sound propagation near to the ground has been investigated extensively [3]. Typically, predictions of outdoor sound propagation characterize the acoustical response of the ground by its specific acoustic impedance which is the ratio of acoustic pressure to air particle velocity at the ground surface. Most impedance models assume that air-saturated ground may be idealized as a porous material in which the solid part is much heavier than the interstitial air and hence may be considered to be motionless. The destructive interference between sound arriving at a receiver after being reflected from the ground and that arriving directly from the source is included in many prediction schemes and is known as ground effect attenuation. The influence of finite impedance ground on the propagation of sound is measured by the excess attenuation which is the attenuation in excess of that expected resulting from wavefront spreading and air absorption. This requires knowledge of the free-field spectrum of the source at the distance of interest. A more convenient measurement in the field is the difference in sound levels between two microphones with a known separation. Once either an excess attenuation or a level difference spectrum is acquired, the frequency-dependent impedance of the surface can be deduced with the aid of sound propagation models [4]. This enables estimates of several pore-related properties such as porosity and air permeability which determine the surface impedance and are impedance model parameters. Although the assumption of a motionless (rigid) porous frame is adequate to explain above-ground sound propagation, it is not suitable for explaining the wave propagation within the ground or the elastic response of ground subjected to the incoming sound from an airborne source. A more detailed account of the use of non-invasive A/S coupling to deduce soil rigidity profiles is available elsewhere [5]. Here, after outlining the approach, some recent results are presented.

1.2 Noise control using rough ground

Ground effect is the interference between travelling directly from source to receiver and sound that arrives at the receiver having been reflected at the ground. Although ground effect is included in many schemes for predicting outdoor sound propagation, little attention has been devoted to the potential for exploiting and optimising ground effect for noise reduction. Most commonly, useful attenuation of surface transport noise is associated with porous (finite impedance) ground that enables sound to penetrate the surface thereby being attenuated and changed in phase during reflection. Roughness that is small compared with the incident wavelength, on ground that would otherwise be acoustically-hard, also results, effectively, in a finite ground impedance over a frequency range determined by the mean roughness height and spacing. After considering the measurements of near-grazing propagation over a comb-like surface composed from parallel strips, ways of designing roughness on hard ground to give significant attenuation of surface transport noise are discussed. Frequency- and time-domain measurements have been made on surfaces composed from parallel periodically- and randomly-spaced rectangular strips (width 0.0126 m, height 0.0253 m) placed on an acoustically-hard surface. Predictions show that a porous layer model is adequate when the spacing is less than the height but a different model is needed otherwise. Only an outline of the work on the generating surface waves as a means of noise control is given here. More details can be found elsewhere [6,7].

2 Parameters from A/S data

2.1 Modelling and Measurements

A widely used method of modelling the physical properties of fluid-saturated poro-elastic materials is the classical theory first published by Biot [8] and subsequently modified by Stoll [9] to model propagation in marine sediments. This predicts that there are three types of elastic waves propagating in a fluid-saturated porous elastic solid: type–I and –II compressional waves and a shear wave. It has been used to explain A/S coupling measurements on soils [10]. It makes two important assumptions about the poroelastic material (i) that it is fully (fluid) saturated and (ii) that its response to the acoustic excitation is linear. The assumption of fluid saturation allows use of a two-phase theory; the two phases being solid and fluid (either gas or liquid). In general soils will contain some water. If the water content is sufficient to enable wave paths through water in addition to those through the solid and air, then a three-phase theory is required [11] which predicts the possibility of an additional compressional wave. A three-phase scenario has been considered in the case of frozen soil [12] and the associated prediction of two shear wave types has been verified experimentally [13]. The sandy soils studied in the present paper are almost never saturated. However, the assumption is made that they may be regarded as fully air-saturated and that any water content serves only to affect the effective elastic moduli rather than creating additional wave types:

The form of Biot-Stoll theory used in deducing soil rigidity profiles introduces several parameters related to the soil grains and the solid frame. These include bulk density, bulk and shear moduli and associated loss factors (assumed to be approximately equal). Other parameters that are introduced relate to the pore structure and include air permeability, porosity and tortuosity. Sophisticated methods of allowing for arbitrary pore microstructure introduce up to seven pore-space-related parameters. The number of fitting parameters related to pore structure is limited here to three by assuming a pore microstructure of tortuous parallel slits.

The propagation paths of incident, reflected and transmitted waves initiated by an above-ground acoustic source are illustrated in Figure 1.

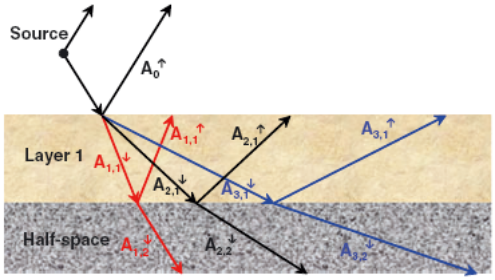

Figure 1 Assumed wave types and paths in a system consisting of a single poroelastic layer over a poroelastic halfspace

The amplitudes of the reflected and transmitted waves within the layered soil are determined for a given source strength by solving a boundary value problem, the complex wave numbers for the three types of waves having been calculated for each poroelastic layer. The solution of the boundary value problem is detailed elsewhere [14, 5].

Information about the soil of interest is obtained non-invasively by measuring the soil particle motion resulting from an incident sound wave using a laser Doppler vibrometer (LDV - Model PSV-200, Polytec, Waldbronn) deployed with the laser beam obliquely incident to the surface. The solid soil particle motion is a consequence of acoustic-to-seismic (A/S) coupling. A compression driver (Model PD-30T, Atlas Sound, Ennis, TX) extended by a metal pipe was used as a monopole acoustic source. The sound field in air was detected by two vertically separated precision microphones (Model 4189, Bruel & Kjær, Nærum). A schematic of the measurement configuration is shown in Figure 2.

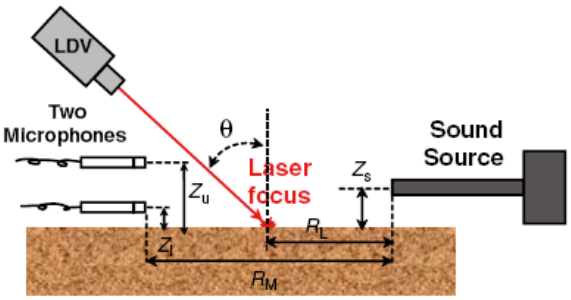

Figure 2 Schematic of the A/S measurement system used for soil parameter deduction

Since soil dynamics are inherently nonlinear, care has been taken to use excitation levels that produced more or less linear responses i.e. only data foud to be independent of the excitation level has ben used. Soil properties have been deduced by comparing predicted and measured acoustic-seismic data. The predictions assume that the soil surface is smooth, or at least that the surface roughness dimensions are significantly smaller than the wavelength at a frequency of interest. The surface is preferably horizontal. The soil is assumed to be horizontally unbounded, but, normal to the surface, the soil is eventually bounded by a rigid half-space, such as a hardpan. Above the hardpan the soil can be composed of several layers. The boundaries of all the layers are assumed to be parallel to one another. Since the measurements employ two microphones and an LDV, three transfer functions are evaluated for each dataset. An optimization algorithm has been run to find a parameter set that minimizes a cost function (CF), determined by the normalized difference of all the measured and the simulated transfer functions (TF) i.e.

$$CF = \sum_{p=1}^{3} \left(\frac{\sum_f \left(|TF_{mea,p}(f)| - |TF_{sim,p}(f)| \right)^2}{\sum_f |TF_{mea,p}(f)|^2} \right) \qquad (1)$$

The subscripts *mea* and *sim* denote measured transfer functions and those simulated using the wave propagation model. The variable f is the frequency, and the subscript p denotes the type of transfer function. Only the magnitudes of complex transfer functions are used since this ensures better con-vergence than use of complex values. This is calculated simultaneously for all parameters thereby necessarily entailing multi-dimensional optimisation. Although standard multi-dimensional opt-imisation algorithms are available for both local and global searching, it has been found best to use a local search algorithm [15]

many times with different initial guesses. A Latin hypercube sampling procedure [16] has been used to ensure that the initial guesses are as uniformly spaced as possible in the multi-dimensional space. Depending on the number of frequencies and optimisation settings included, the search takes between several hours and several days using a state-of-art desk top computer.

2.2 Results for soil strength profiles

Results that assumed a fixed hard-pan depth, made use of initial estimates of porosity and permeability from fitting acoustic level difference spectra [17 Hess et al 1990] and based on measurements made in an area that was clear from crops have been published elsewhere [5]. Here are presented field data collected in 2013 inside crops at the Rothamsted experimental facility at Woburn, Beds. UK using geometries listed in Table 1.

Table 1 Geometries used in A/S measurements on soils (see Fig. 3)

Site/ Day	Horizontal distances/mm		heights /mm		LDV beam ° from normal
Paragon #3					
Day 1	Source to Upper Mic	443	Source	114	36
	Source to Lower Mic	450	Upper mic	152	
	Source to LDV spot	246	Lower mic	48	
Day 2	Source to Upper Mic	434	Source	104	37
	Source to Lower Mic	434	Upper mic	163	
	Source to LDV spot	274	Lower mic	67	
Day 3	Source to Upper Mic	492	Source	82	31
	Source to Lower Mic	496	Upper mic	115	
	Source to LDV spot	329	Lower mic	15	
Hystar #52					
Day 3	Source to Upper Mic	267	Source	116	31
	Source to Upper Mic	264	Upper mic	115	
	Source to Upper Mic	210	Lower mic	12	

Figure 3 compares A/S deduced rigidity modulus as a function of depth with penetrometer data taken at the same sites but only those in Fig. 3(a) were obtained on the same day (Day 1) as A/S measurements. In the parameter deduction optimisation, several runs were made assuming that up to 4 layers were present above the underlying half space. The A/S deduced shear wave speeds do not use initial estimates of porosity and permeability from level difference spectra since the scattering by vegetation made these spectra difficult to fit over a wide frequency range. Examples of measured and fitted A/S TF spectra are shown in Fig. 4.

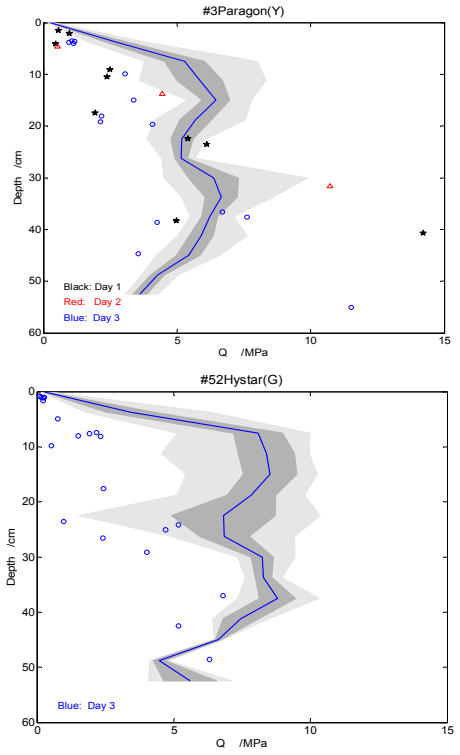

Figure 3 Mean (blue lines) and spread (grey areas) of penetrometer resistance profiles measured at two locations compared to profiles (points) deduced from A/S data (a) Paragon #3 site: Black stars – 27 June 2013, red squares 8th July 2013, blue circles 6th August 2013 (b) Hystar #52 6th August 2013.

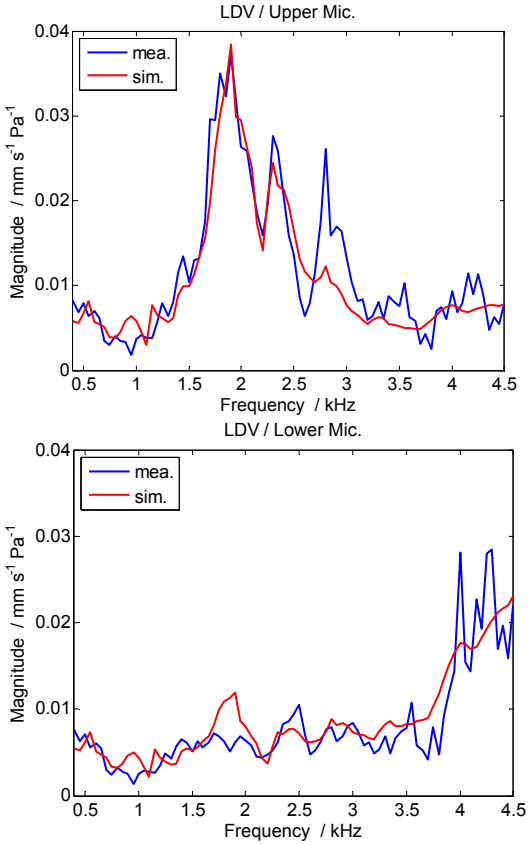

Figure 4 Example comparisons between measured A/S transfer function spectra (blue curves) obtained at Woburn compared with predictions using fitted parameters (red curves).

The deduced rigidity moduli (μ) have been converted to penetrometer resistance (Q) using the empirical relationship [18]:

$$Q/\mu = 2.87 \times 10^{-2} \quad (2)$$

The blue lines represent the means of the penetrometer resistance readings taken at the same sites but only some of those shown in Fig.3(a) were obtained on the same day as some of the A/S data. The darker and narrow grey regions represent the standard errors; the lighter and wider grey regions show the maximum and minimum of the readings at each depth. The discrete markers in the figures indicate the rigidity of each deduced layer at its centre. In Fig. 3(a) two sets of fitted layer depths and soil rigidity deductions are shown for Day 3.

3 Propagation over rough ground

3.1 Surface waves over roughness

Coherent scattering of sound waves from a rough surface has been studied extensively. A convenient method for predicting propagation over artificially created rough surfaces, including surfaces composed of periodically spaced roughness elements is the 'boss' model. Tolstoy [19, 20] described the 'boundary waves' produced due to energy trapping between the roughness elements and formulated stochastic and boss models which do not include incoherent scatter and according to which the predicted effective impedance of a rough hard surface is purely imaginary. Medwin *et al* [21] carried out experiments on surface waves over artificially rough boundaries using microphones flush with the rough surface with the intention of measuring boundary waves and comparing them with predictions of Tolstoy's models. The predictions were found to over-estimate the amplitude of the surface wave component. A theory due to Twersky [22, 23] includes incoherent scatter but has been found to need modification at low frequency to allow for penetrable scatterers [24]. Nevertheless it has been found possible to represent rough surface coherent scattering data obtained in the laboratory by an effective impedance [25].

.

3.2 Theory

A comb-like surface is expected to be locally-reacting and to have purely imaginary normalised impedance given by

$$Z(L)/\rho c = \coth(-ikL) \quad (3)$$

where L is the layer thickness and $k = \omega/c$ is the wave number in air, ω being angular frequency and c the adiabatic sound speed.

Ultrasonic surface waves over rectangular grooves have been analysed using a modal theory deduced from studies of em wave propagation [26] The theory indicates the existence of additional surface waves associated with higher order harmonics but these are highly damped.

When centre-to-centre separation $d \ll \lambda$ between rectangular grooves with width a and depth L,

$$k(L)/k = (a/d)\coth(-ik(L - a\log(2)/\pi)). \quad (4)$$

This vertical propagation constant includes a factor of porosity ($\Omega = a/d$) and implies an effective layer thickness of ($L - a\log(2)/\pi$) i.e. the effective depth of the layer is less than the actual depth. The corresponding expression for the normalised horizontal wave number is

$$k(x)/k = \sqrt{1 + (a/d)^2 \tan^2 k(L - a\log 2/\pi)} \quad (5)$$

A surface wave is known to be created in the vicinity of the surface of a thin porous layer and is associated with an imaginary part (reactance) of the surface impedance that is greater than the real part (resistance). A comb-like (periodically-rough) hard surface may be considered to be a hard-backed locally-reacting rigid porous layer composed of slit-like pores. Analytical expressions for the corresponding acoustical properties [3] allow for viscous and thermal losses inside the slit-like pores (see equations (6) – (8)).

$$\lambda = \sqrt{\frac{3\omega\rho_o T}{\Omega R_s}} \quad (6a)$$

$$H(\lambda) = 1 - \frac{\tanh(\lambda\sqrt{-i})}{(\lambda\sqrt{-i})} \quad (6b)$$

$$\rho_c(\lambda) = \frac{\rho_o}{H(\lambda)} \quad (6c)$$

$$C_c(\lambda) = (\gamma P_o)^{-1}\left(\gamma - (\gamma - 1)H\left(\lambda\sqrt{N_{PR}}\right)\right) \quad (6d)$$

where Ω is the porosity, R_s is the flow resistivity, T is the tortuosity, γ is the ratio of specific heats N_{PR} is the Prandtl number, ρ_0 is the density (all for air), P_0 is atmospheric pressure, $\rho_c(\lambda)$ is the complex density and $C_c(\lambda)$ is the complex compressibility.

The characteristic impedance Z_c and propagation constant k_c are given by eqns. (7) and (8) respectively.

$$Z_c(\omega) = \frac{1}{\rho_o c_o}\sqrt{\frac{T}{\Omega^2}\frac{\rho_c(\lambda)}{C_c(\lambda)}} \quad (7)$$

$$k_c(\omega) = \omega\sqrt{T\rho_c(\lambda)C_c(\lambda)} \quad (8)$$

Much previous research on acoustical propagation over periodically-rough surfaces has focused on surface wave creation [27] and on time domain data rather than on frequency domain information such as excess attenuation (EA) or insertion loss (IL) spectra. The latter are important in the context of designing rough surfaces for noise control and for predicting the effective impedance of rough outdoor surfaces for use when predicting outdoor sound propagation.

The EA is calculated using

$$EA = 20\log\left(\frac{P_{total}}{P_{direct}}\right) \quad (9)$$

where P_{total} is the total pressure received at the microphone including the direct and reflected waves from the ground surface (see eqn.(10a)) and P_{direct} is the pressure due to the direct wave from a point source (see eqn. (10b)).

$$P_{total} = \frac{Pe^{ikR_1}}{R_1} + \frac{QPe^{ikR_2}}{R_2}, P_{direct} = \frac{Pe^{ikR_1}}{R_1} \quad (10a.b)$$

where Q is the spherical wave reflection coefficient, R_1 is the direct path length from source to receiver and R_2 is the reflected path length through the specular reflection point.

Combining eqns. (9) and (10) gives,

$$EA = 20\log\left(1 + \frac{R_1 Q e^{ik(R_2 - R_1)}}{R_2}\right) \quad (11)$$

The excess attenuation predictions use equations (12-13) for the complex reflection coefficient which assume local reaction.

$$Q = R_p + (1 - R_p)F(w) \quad (12)$$

where R_p is the plane wave reflection coefficient, $F(w)$ is the boundary loss factor, w is the numerical distance

$$R_p = \frac{\cos\theta - \beta}{\cos\theta + \beta} \quad (13a)$$

$$F(w) = 1 + i\sqrt{\pi} w e^{-w^2} erfc(-iw) \quad (13b)$$

$$w = \sqrt{\frac{ikR_2}{2}}(\cos\theta + \beta) \quad (13c)$$

β is the normalised surface admittance and θ is the angle of incidence.

3.3 Laboratory measurements and predictions

Measurements have been made of sound propagation over several arrays of small rectangular aluminium strips ((width 0.0126 m, height 0.0253 m) spaced at equal intervals between 0.003 m and 0.0674 m on varnished medium density fibreboard (MDF) [Bashir et al 2013]. The strip locations were centred on the point of specular reflection which was halfway between source and receiver when they were at equal heights. Figure 5 shows two example configurations of aluminium strips with and without absorbing material at the strips ends. A Tannoy® driver fitted with a 2 m long tube, of 3 cm internal diameter was used as a point source and a Bruel & Kjaer® type 4311 ½-inch-diameter condenser microphone fitted with a preamplifier was used as a receiver. Both source and receiver were placed at equal heights of 0.045 m (i.e. approximately 2 cm above the top of the strips) and at a horizontal separation of 0.7 m. A data acquisition system based on maximum length sequence (MLS) was used for signal generation and signal processing. The background noise in the received microphone signals has been removed by correlation with the known output sequence. The free field data needed for calculating excess attenuation spectra were obtained by raising source and receiver to a height of 2 m above the grid floor of the anechoic chamber so that unwanted reflections were minimized.

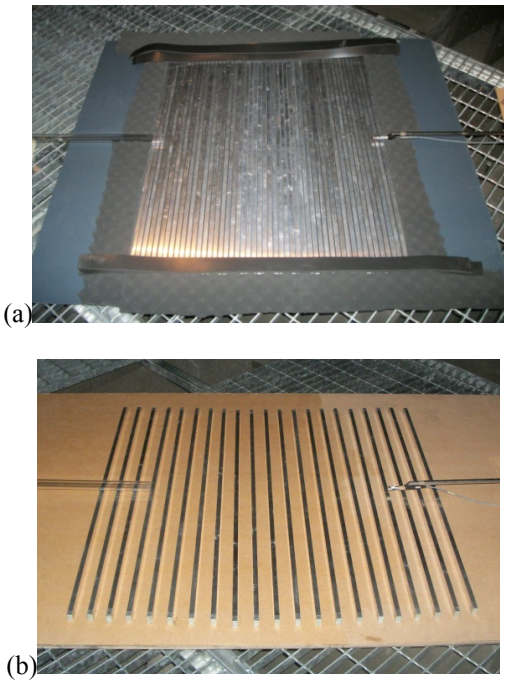

Figure 5 Laboratory arrangements for frequency and time domain measurements over 1 m long parallel aluminium strips (width 0.0126 m, height 0.0253 m) located on an MDF board with edge-to-edge spacing of (a) 0.003 m and (b) 0.0474 m. In (a) the ends of the strips are 'terminated' by absorbing materials

Figure 6 compares measured time domain signals when the edge-to-edge spacing was 0.0124 m without and with absorbing materials placed at the strip ends. Without the absorbing material the finite lengths of strips generate additional waves which interfere with the main pulse. The additional waves behave like surface waves and attenuate with increase in receiver height but their main frequency content is higher than of the surface waves of interest here. The absorbing material at the strip ends reduces these additional waves considerably but not completely.

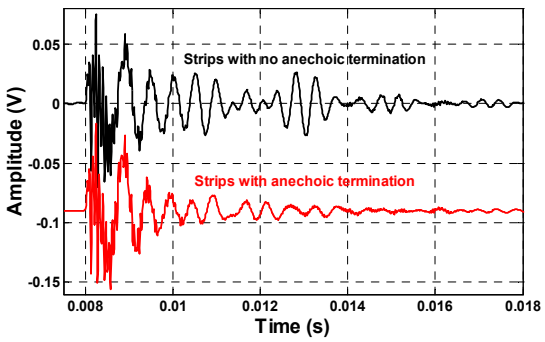

Figure 6 Measured time domain signals for source and receiver at heights of 0.045 m, separated by 0.7 m over aluminium strips placed with edge-to-edge spacing of 0.0124 m without and with absorbing materials at the strip ends.

Figure 7 (a) compares time domain signals obtained at different receiver heights between 0.03m and 0.15m m over a surface composed of 50 aluminum rectangular strips with edge-to-edge spacing of 0.0124 m and with the center of the source tube located at a height of 0.045 m from MDF board i.e. 0.02 m above the aluminum strips. The waveforms corresponding to the lower receiver heights show a strong surface wave, whereas there is little or no surface wave when the receiver is in the higher location. This is consistent with the exponential decrease with height in a surface wave.

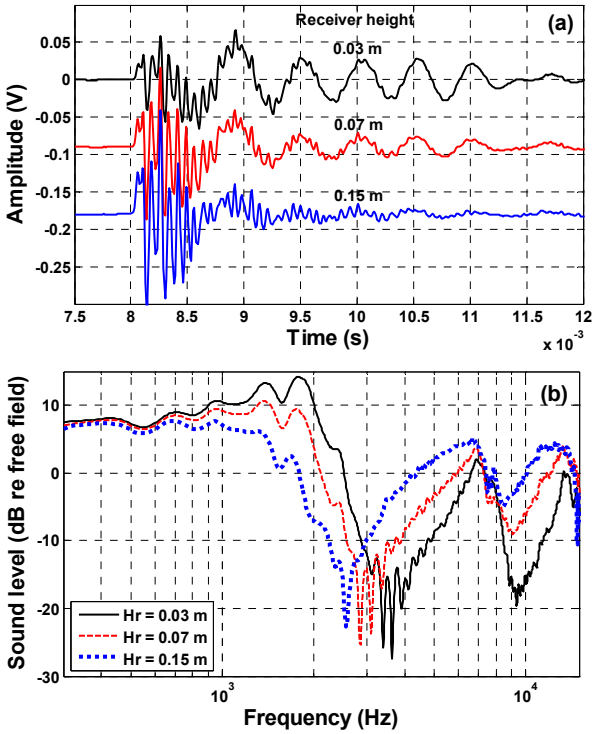

Figure 7 (a) Time domain data obtained over aluminium strips placed on MDF board with edge-to-edge spacing of 0.0124 m at different receiver heights of 0.03 m, 0.07 m and 0.15 m, source at height of 0.045 m and with source-receiver separation of 0.7 m (b) corresponding excess attenuation spectra. The source and receiver heights are measured with respect to the MDF board base.

These characteristics are confirmed by Figure 7 (b) which shows measured excess attenuation spectra obtained with source and receiver separated by 0.7 m above a surface containing rectangular strips with edge-to-edge spacing of 0.0124 m and receiver heights between 0.03 m and 0.015 m. The presence of a surface wave is indicated by values of EA > 6 dB near 2 kHz. Figure 7 (b) indicates that the strength of the surface wave depends on the source and receiver heights. There is a strong surface wave when the receiver is at height of 0.03 m but little or no surface wave when the receiver is at a height of 0.15 m.

Predictions of excess attenuation spectra have been made using (a) a 2D Boundary Element Method (BEM) and (b) by assuming a slit pore layer impedance of the 'surface' formed by the strips [Attenborough et al 2007]. The BEM predictions are improved if the MDF base is assumed to have finite impedance. Measurements of EA spectra over the board alone have shown that the MDF impedance can be modelled by a two-parameter variable porosity model with an effective flow resistivity 10 MPa s m^{-2} and an effective porosity rate 1.0 m^{-1}. The porosities of the strip configurations used in the slit pore layer predictions are deduced from the width of the aluminium strips and their spacing (see Table 2).

Table 2 Properties of aluminium strip arrays when considered as slit-pore layers.

Edge-to-edge-spacing m	**porosity**	**Flow resistivity Pa s m^{-2} from eqn. (12)**
0.0030	0.190	127.0
0.0674	0.843	0.06

The flow resistivity is calculated from these values of porosity (Ω) and equation (14)

$$R_s = \frac{2\mu s_o T}{\Omega r_h{}^2} \qquad (14)$$

in which, for the slit-like pores between the strips, the steady flow shape factor s_0 = 1.5, the hydraulic radius r_h is the semi-width of a slit and the tortuosity (T) is assumed to be unity.

Figures 8(a) and (b) show the dependence of measured and predicted EA spectra on strip spacing. The BEM gives good predictions for both edge-to-edge spacings despite residual effects particularly in the first EA minimum from the finite lengths of the strips. The slit-pore layer impedance model with an effective layer depth of 0.027 m (slightly larger than the strip height of 0.0253 m) gives accurate predictions as long as the edge-to-edge spacing is 0.015 m or less but its predictions deteriorate progressively as the edge-to-edge spacing of the strips is increased beyond 0.015 m.

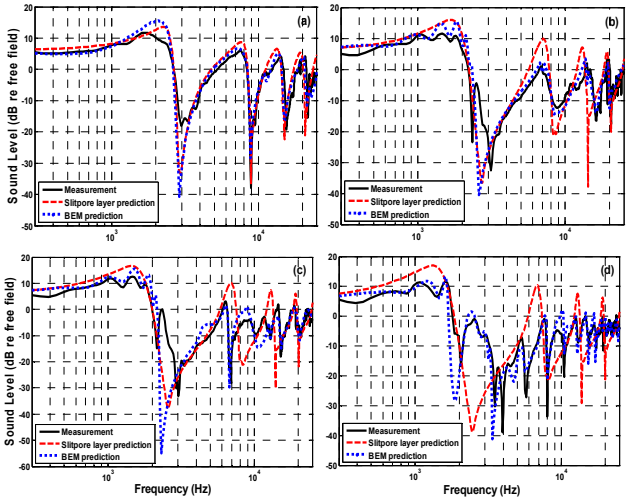

Figure 8 Excess attenuation spectra measured (black continuous lines) with source and receiver at a height of 0.045 m above an MDF board surface and 0.7 m separation over 0.0253 m high aluminium strips placed on the board with edge-to-edge spacing of (a) 0.0030 m (b) 0.0124 m (c) 0.0274 m and (d) 0.0674 m. Also shown are BEM calculations (dotted lines) and predictions assuming slit-pore layer impedance (dashed lines) with effective layer depth 0.027 m. The parameter values used for the slit-pore predictions (red broken lines) are listed in Table 2. BEM predictions (blue dotted line) assume that the MDF board impedance is given by the 2-parameter variable porosity model [3] with effective flow resistivity 10 MPa s m^{-2} and effective porosity rate 1.0 m^{-1}.

3.4 Surface wave generation and outdoor noise control

Figures 9(a) and (b) respectively show a 2.3 m wide 16 m array of long low parallel walls and a lattice made by stacking pairs of bricks (dimensions 21.5 cm length, 10 cm width and 6.5 cm height). Figures 10(a) and (b) show the corrsponding sound level spectra measured during drive by tests without the walls and with the walls at 2.5 m from the nearest vehicle wheels [7].

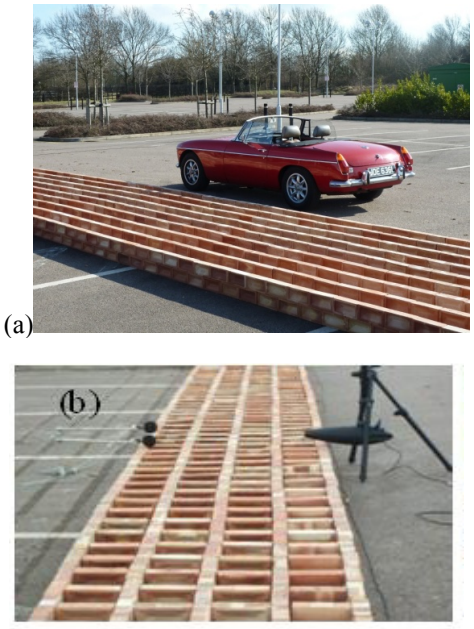

Figure 9 (a) 2.3 m wide 16 m long low parallel brick wall configuration and (b) 1.1 m wide brick lattice used in drive by measurements [7].

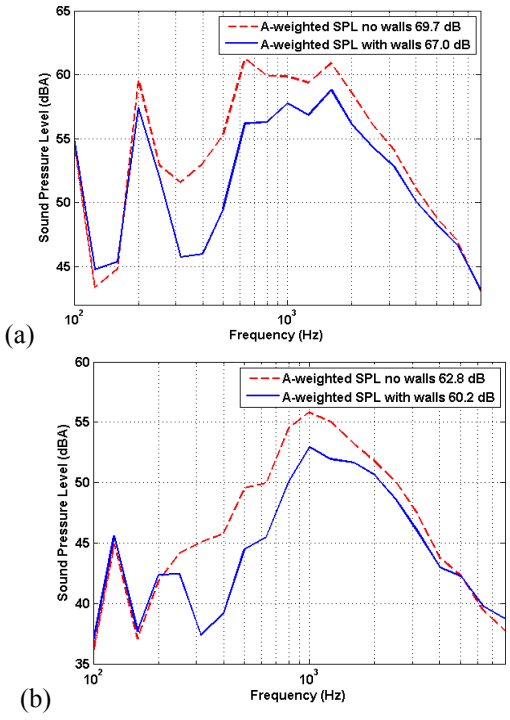

Figure 10 Sound level spectra measured at the closest point of approach during drive by tests (different cars) without and with the wall configurations shown in Figures 9(a) and 9(b) respectively.

Each curve represents the average of levels recorded during five pass-bys. The average pass-by speed of was 35.4 km/h. The corresponding broadband insertion losses at a 1.5 m high receiver 10 m from the nearest wheels were nearly 3 dB. The fact that the SPL measured between 100 Hz and 200 Hz with the parallel walls present is higher than without the walls (Fig. 10(a)) indicates that a surface wave is generated by the parallel walls and thereby energy is redistributed from higher frequencies. The 1.1 m wide square cell lattice wall configuration resulted in more or less the same overall broadband reduction in the noise from car 2 as did the 2.14 m wide nine parallel walls configuration for car 1 while occupying significantly less land.

3.5 Effective impedance of a brick lattice

A (2D) BEM cannot be used directly to predict propagation over 3D arrangements such as the lattice. It would be coneveient if the acoustical effects of such surfaces could be represented by their *effective surface impedance*. This can be deduced from measurements of the received signals due to a point source. Excess attenuation data obtained with point source loudspeaker and vertically-separated microphones over a lattice array (see Fig. 9(b)) have been compared with predictions using a model for the impedance of a slit pore layer with effective flow resistivity = 400 Pa·s·m^{-2}, porosity = 0.55, tortuosity = 1.0 and effective layer depth = 0.25 m. Figure 11 compares a measured level difference spectrum with a spectrum predicted using this effective impedance. The good fit between predictions and data for these geometries means that the effective slit pore layer impedance can be used with the classical formulae for propagation from a point source over a finite impedance boundary (see equations (11) to (13)) to predict propagation over a (continuous) lattice for other geometries.

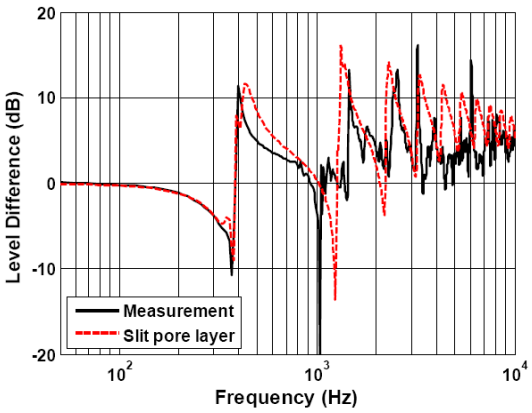

Figure 11. Comparison of a measured level difference spectrum (source height = 0.1m, upper microphone height = 0.15m, lower microphone height = 0.05m, horizontal separation = 2m) above a 0.2 m high brick lattice on a car park with the spectrum predicted by assuming a point source above a slit pore layer impedance with flow resistivity = 400 Pa s m-2, porosity = 0.55, tortuosity = 1.0 and (effective) layer depth = 0.25 m.

3.6 Effect of a gap in the lattice

Gaps can cause significanht deterioration in the acoustical performance of a conventional traffic noise barrier. However this is not the case with ground treatments used for noise control. Figure 12 shows a 0.2 m high 8.6 m long 1.79 m wide brick lattice containing a 0.4 m wide path normal to the line of a drive by test. Averaged insertion losses (3 pass-bys at an average speed of 41.0 km/h without a path and 4 passbys at an average speed of 45 km/h with a path) are detailed in Table 3. The creation of the path results in a small reduction (about 0.5 dB) in insertion loss.

Table 3: Averaged sound pressure levels and insertion losses during drive by tests next to an 8.6 m long 2.30 m wide brick lattice (Figure 12) without and with a central 0.4 m wide path.

	A-weighted SPL no walls (dB)	A-weighted SPL with walls (dB)	Insertion loss (dB)
No path	64.2	62.0	2.2
With path	64.2	62.4	1.8

4. Concluding Remarks

Two uses of sound waves generated near porous and rough surfaces have been described. Acoustic-to-seismic coupling can be used for monitoring of soil rigidity profiles that are important for plant growth. The associated parameter fitting is computationally demanding but the method is non-invasive and is capable of yielding information in soil conditions and to depths that are inconvenient and difficult using traditional soil techniques. The generation and attenuation of surface waves by roughness on (otherwise) acoustically-hard boundaries can be used for surface transport noise reduction. This offers a useful option for of noise control where the use of conventional barriers is inappropriate and where access is important.

Acknowledgements

The research leading to these results has received funding from the Engineering and Physical Sciences Research Council (UK) grant ref. EP/H040617/1 and the European Community's Seventh Framework Programme (FP7/2007-2013) under grant agreement n° 234306, collaborative project HOSANNA.

References

[1] N. Harrop, and K. Attenborough, Laser-Doppler vibrometer measurements of acoustic-to-seismic coupling in unconsolidated soils. *Applied Acoustics*, **63**, 419–429 (2002).

[2] N. Xiang, and J. M. Sabatier, An experimental study on antipersonnel landmine detection using acoustic-to-seismic coupling. *Journal of the Acoustical Society of America*, **113**, 1333–1341 (2003).

[3] K. Attenborough, K. M. Li, and K. Horoshenkov,. *Predicting Outdoor Sound*. Taylor & Francis, London (2007).

[4] S. Taherzadeh, S. and K. Attenborough, K. Deduction of ground impedance from measurements of excess attenuation spectra. *Journal of the Acoustical Society of America*, **105**, 2039–2042 (1999).

[5] H. C. Shin, S. Taherzadeh, K. Attenborough, C. Watts and R. Whalley, Non-invasive characterization of pore-related and elastic parameters of soils in linear Biot-Stoll theory and acoustic-to-seismic coupling, *European Journal of Soil Science*, **64** 308 – 323 (2013).

[6] I. Bashir, S. Taherzadeh and K. Attenborough., Surface waves over periodically-spaced strips. *Journal of the Acoustical Society of America.* **134** (6) 4691 – 4697 (2013).

[7] I. Bashir, T. Hill, S. Taherzadeh, K. Attenborough K. and M. Hornikx, Reduction of Surface Transport Noise by Ground Roughness, submitted to *Applied Acoustics* (2014).

[8] M. A. Biot. Theory of propagation of elastic waves in a fluid-saturated porous solid. I. Low-frequency range, II. Higher frequency range. *Journal of the Acoustical Society of America*, **28**, 168–191 (1956).

[9] R. D. Stoll, Acoustic waves in marine sediments in *Physics of Sound in Marine Sediments*, ed. L. Hampton pp. 19 – 39 Plenum Press, New York (1974).

[10] J. M. Sabatier, K. Attenborough, H. E. Bass and L. N. Bolen, Acoustically-induced Seismic Waves *Journal of the Acoustical Society of America* **80** (2) 646-649

[11] W. Brutsaert, The propagation of elastic waves in unconsolidated unsaturated granular mediums, *J. Geophys. Res*. **69** 243 – 257 (1964).

[12] P. Leclaire, F. Cohen-T´enoudji and J. Aguirre-Puente, Extension of Biot's theory of wave propagation to frozen porous media. *Journal of the Acoustical Society of America*, **96**, 3753–3768 (1994).

[13] P. Leclaire, F. Cohen-T´enoudji and J. Aguirre-Puente, Observation of two longitudinal and two transverse waves in a frozen porous medium. *Journal of the Acoustical Society of America*, **97**, 2052–2055, (1995).

[14] S. Tooms, S. Taherzadeh, and K. Attenborough, Sound propagation in a refracting fluid above a layered fluid-saturated porous elastic material. *Journal of the Acoustical Society of America*, **93**, 173–181 (1993).

[15] H. Rosenbrock,. An automatic method for finding the greatest or least value of a function. *Computer Journal*, **3**, 175–184 (1960).

[16] A. I. J. Forrester,.A. S´obester, and A. J. Keane. *Engineering Design via Surrogate Modelling: A Practical Guide*. John Wiley & Sons, Chichester (2008).

[17] H. M. Hess, K. Attenborough and N. W. Heap, Ground characterization by short-range propagation measurements. *Journal of the Acoustical Society of America*, **87**, 1975–1986 (1990).

[18] W. Gao, C. Watts, T. Ren, H-C. Shin, S. Taherzadeh, K. Attenborough,. M. Jenkins, and W. R. Whalley, Estimating Penetrometer Resistance and Matric Potential from the Velocities of Shear and Compression Waves, *Soil Science Society of America Journal* (2013), doi 10.2136/sssaj2012.0394, Table 6

[19] I. Tolstoy, Coherent sound scatter from a rough interface between arbitrary fluids with particular reference to roughness element shapes and corrugated surfaces, *Journal of the Acoustical Society of America*. **72,** 960 – 972 (1982).

[20] I. Tolstoy, Smoothed boundary conditions, coherent low-frequency scatter, and boundary modes, *Journal of the Acoustical Society of America*, **72,** 1 – 22 (1983).

[21] H. Medwin, G. L. D'Spain, E. Childs and S. J. Hollis, Low-frequency grazing propagation over periodic steep-sloped rigid roughness elements, *Journal of the Acoustical Society of America*, **76,** 1174 – 90 (1984).

[22] V. Twersky, Reflection and scattering of sound by correlated rough surfaces, *Journal of the Acoustical Society of America*, **73,** 85 – 94 (1983)

[23] R. J. Lucas and V. Twersky, Coherent response to a point source irradiating a rough plane, *Journal of the Acoustical Society of America*, **76,** 1847 – 63 (1984).

[24] P. Boulanger, K. Attenborough, S. Taherzadeh, T. Waters-Fuller and K. M. Li, Ground Effect Over Hard Rough Surfaces, *Journal of the Acoustical Society of America*, **104,** 1474 – 82 (1998).

[25] P. Boulanger, K. Attenborough and Q. Qin, Effective impedance of surfaces with porous roughness: Models and data, *Journal of the Acoustical Society of America*, **117(3)** 1146 – 1156 (2004).

[26] L. Kelders, J. F. Allard and W. Lauriks, Ultrasonic surface waves above rectangular-groove gratings, *Journal of the Acoustical Society of America*, **103,** 2730 – 2733 (1998).

[27] G. A. Daigle, M. R. Stinson, and D. I. Havelock, Experiments on surface waves over a model impedance plane using acoustical pulses, *Journal of the Acoustical Society of America*, **99** (4)**,** 1993 – 2005 (1996).